Resolution improvement with dispersion manipulation and a retrieval algorithm in optical coherence tomography

I-Jen Hsu, Chia-Wei Sun, Chih-Wei Lu, C. C. Yang, Chun-Ping Chiang, and Chii-Wann Lin

We propose and demonstrate what is to our knowledge a novel technique of improving the spatial resolution of an optical coherence tomography (OCT) system given a non-Gaussian light source spectrum. By using dispersive materials in the reference arm of the OCT system, the resultant dispersion variation led to a full-width at half maximum (FWHM) of the interference fringe envelope smaller than the Fourier transform-limited value of a Gaussian spectral shape with the same spectral FWHM, at the expense of significant tails. The effects of the tails, which would blur the OCT images, were tremendously reduced with a retrieval algorithm. Simulation results and processed OCT scanning images have shown the capability of the proposed technique.

OCIS codes: 170.4500, 100.3010.

1. Introduction

Optical coherence tomography (OCT) has been proved useful for biomedical imaging applications.[1] Currently, its development directions include higher spatial resolution, higher sensitivity, faster scanning, functioning imaging, deeper scanning, Doppler tomography, endoscopy applications,[2,3] etc. For higher axial resolution, broadband light sources for OCT are required. A larger bandwidth leads to a higher axial resolution. So far, the applied broadband sources include semiconductor-based superluminescence diodes with the spectral width up to 80 nm centered at 1310 nm,[4] extremely short Ti:sapphire laser pulses with the spectral width up to 350 nm centered at 800 nm,[5] nonlinear-optics broadened spectra in a tapered fiber or photonic crystal fiber,[6,7] and a superluminescent light source using a Ti:Al_2O_3 crystal pumped by a frequency-doubled diode pumped laser.[8]

Although the full-width at half maximum (FWHM) of the interference fringe envelope is usually used for defining the axial resolution of an OCT system, a light source with non-Gaussian spectral shape will usually produce the effects of sidelobes and tails in the interference fringe envelope that may blur the images. If the effects of the tails or sidelobes can be reduced through a certain signal-processing algorithm, OCT resolution can be improved by reducing the FWHM of the interference fringe envelope through dispersion compensation in one of the interferometer arms.[9] There are several signal-processing methods that have been used to increase the resolution of OCT images, such as deconvolution with a constrained iterative restoration algorithm[10,11] and reduction of the sidelobes with a spectral-shaping technique.[12]

In this paper, we propose and demonstrate what is to our knowledge a novel method for improving OCT axial resolution based on dispersion manipulation and a signal-processing algorithm. With the light source FWHM spectral width of 100 nm centered at 780 nm, the FWHM of the interference fringe envelope is 2.68 μm if the spectrum is Gaussian distributed and the dispersion is balanced. However, with dispersion manipulation the available non-Gaussian spectral distribution resulted in a fringe envelope of only 1.7 μm in FWHM with a significant tail-

I-Jen Hsu, Chia-Wei Sun, Chih-Wei Lu, and C. C. Yang are with the Department of Electrical Engineering and Graduate Institute of Electro-Optical Engineering, National Taiwan University, 1, Roosevelt Road, Section 4, Taipei, Taiwan. Chun-Ping Chiang is with the Department of Dentistry, National Taiwan University, Taipei, Taiwan. Chii-Wann Lin is with the Graduate Institute of Bioengineering, National Taiwan University, Taipei, Taiwan. E-mail address for C. C. Yang is ccy@cc.ee.ntu.edu.tw.

Received 3 June 2002; revised manuscript received 16 September 2002.

0003-6935/03/020227-08$15.00/0

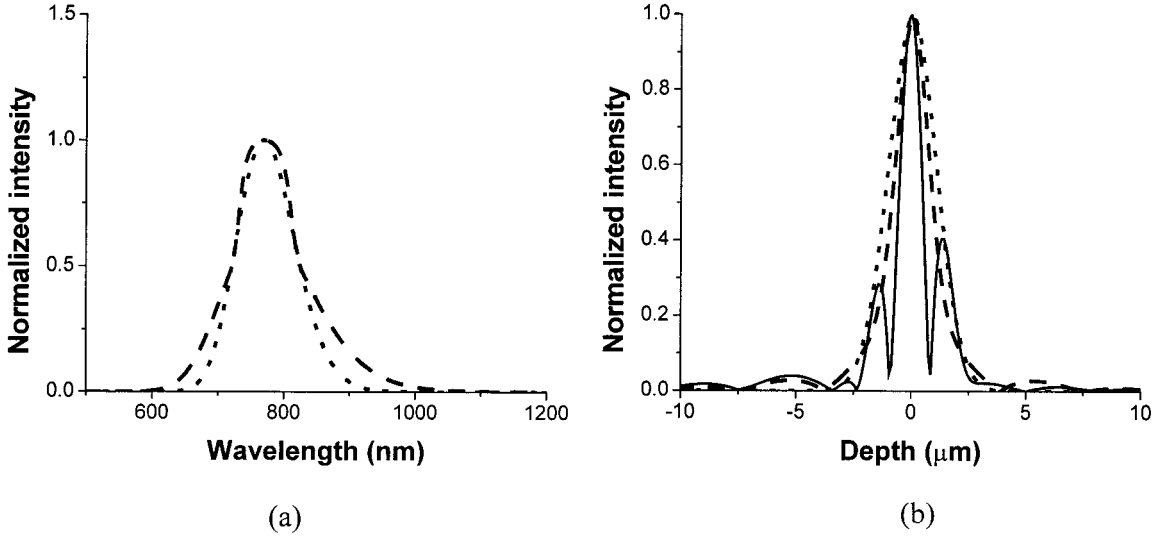

Fig. 1. (a) A non-Gaussian spectrum (dashed curve) and a Gaussian spectrum (dotted curve) with the same FWHM; (b) the resultant interference fringe envelopes of the non-Gaussian (dashed curve) and Gaussian (dotted curve) cases. The solid curve depicts the result when a dispersion mismatch is included.

intensity distribution. The effects of tails in OCT scanned images are significantly reduced with an image-retrieval algorithm. With such a process, image quality is significantly improved. In Section 2 of this paper, the principles of dispersion manipulation for Gaussian and non-Gaussian spectra are discussed. Our experimental procedures are presented in Section 3. The retrieval algorithm is described in Section 4. The results of image-quality improvement are shown in Section 5. Last, conclusions are drawn in Section 6.

2. Relationship between OCT Resolution and Spectral Shape and Dispersion Mismatch

If the spectral intensity of a light source is Gaussian distributed and the dispersion is balanced between the reference and sample arms of the interferometer, the FWHM of the axial resolution cell, Δz, is related to the FWHM of the source spectrum, $\Delta\lambda$, through[13]

$$\Delta z = \frac{2\ln(2)}{\pi}\frac{\lambda^2}{\Delta\lambda}. \tag{1}$$

Here, λ is the center wavelength of the light source. In the case of a non-Gaussian spectral shape, the FWHM of the autocorrelation function, i.e., the interference fringe of an OCT system, can be larger or smaller than the value given in Eq. (1), depending on the intensity distribution of the source spectrum and the dispersion mismatch between the reference and the sample arms of the interferometer. If we consider a Gaussian spectrum with the spectral function $S(\omega)$ as

$$S(\omega) = S_0 \exp\left[-\frac{(\omega-\omega_0)^2}{\Delta\omega^2}\right]. \tag{2}$$

Here, S_0 represents the spectral amplitude, ω_0 denotes the central frequency, and $\Delta\omega$ is related to the spectral width. The wave field $E(t)$ can be expressed as the inverse-Fourier transform of the spectrum

$$E(t) = \frac{1}{2\pi}\int_{-\infty}^{\infty} S(\omega)\exp[j\varphi(\omega)]\exp(j\omega t)\mathrm{d}\omega,$$
$$= \frac{S_0\Delta\omega}{2\sqrt{\pi}}\exp\left(-\frac{\Delta\omega^2 t^2}{4}\right)\exp(j\omega_0 t). \tag{3}$$

Here, $\varphi(\omega)$ represents the frequency-dependent phase and is assumed to be a constant (zero) here in a chirp-free pulse. When the dispersion is balanced between the reference and the sample arms, the autocorrelation function $\Gamma(\tau)$ is

$$\Gamma(\tau) = \int_{-\infty}^{\infty} E_1(t)E_2^*(t+\tau)\mathrm{d}t$$
$$= \frac{{S_0}^2\Delta\omega}{2\sqrt{2\pi}}\exp\left(-\frac{\Delta\omega^2\tau^2}{8}\right)\exp(-j\omega_0\tau). \tag{4}$$

Here, E_1 and E_2 stand for the signals in the reference and the sample arms (assuming an equal amplitude S_0), respectively, and τ denotes the time delay between the two arms. When a dispersion mismatch, $\Delta\varphi(\omega)$, exists as (assuming a and b real)

$$\Delta\varphi(\omega) = a\omega^2 + b\omega, \tag{5}$$

the autocorrelation function becomes

$$\Gamma(\tau) = \int_{-\infty}^{\infty} E_1(t)E_2^*(t+\tau)\mathrm{d}t,$$
$$= \frac{1}{2\pi}\int_{-\infty}^{\infty} |S(\omega)|^2\exp[j\Delta\varphi(\omega)]\exp(-j\omega\tau)\mathrm{d}\omega,$$
$$= \frac{{S_0}^2\Delta\omega}{2[\pi(2-j\Delta\omega^2 a)]^{1/2}}\exp(\alpha), \tag{6}$$

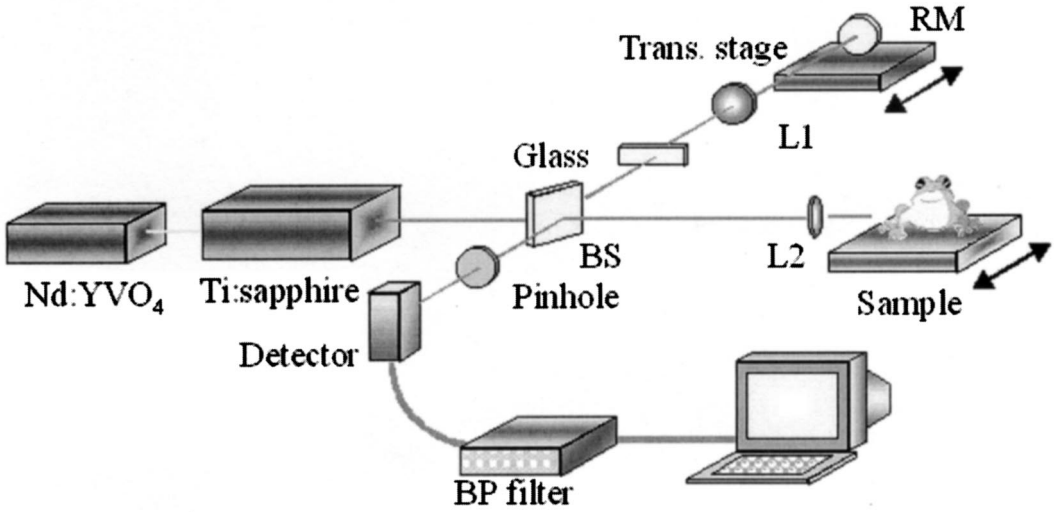

Fig. 2. Experimental setup of the free-space OCT system: BS, beam splitter; L_1 and L_2, lenses; RM, reflection mirror; BP filter, bandpass filter.

where

$$\alpha = -\frac{[\Delta\omega^2(\tau - b) + 4j\omega_0]^2}{4\Delta\omega^2(2 - j\Delta\omega^2 a)} - \frac{2{\omega_0}^2}{\Delta\omega^2}. \tag{7}$$

Note that a in Eq. (5) describes group-velocity dispersion due to the dispersion mismatch and b simply results in a temporal shift. From Eq. (7) one can see that the width of $|\Gamma|$ increases with the value of a. In other words, dispersion mismatch reduces the OCT resolution. Certain dispersion compensation can improve the resolution.

In the case of a non-Gaussian spectral shape, the width of the autocorrelation function can be smaller than that of the Gaussian shape with the same spectral FWHM. In this situation, an appropriate dispersion mismatch may help in further reducing the FWHM of the autocorrelation function at the expense of sidelobe generation. To demonstrate such a possibility, we show an example with a non-Gaussian spectral shape. Figure 1(a) shows a normalized non-Gaussian spectrum (dashed curve) with the spectral density function as

$$|S(\omega)|^2 = 2\,\exp\left[-\frac{(\omega - \omega_0)^2}{{\Delta\omega_1}^2}\right] + \exp\left[-\frac{(\omega - \omega_0)^6}{{\Delta\omega_2}^6}\right]. \tag{8}$$

Here, $\omega_0 = 2.45 \times 10^{15}$ Hz, $\Delta\omega_1 = 3 \times 10^{14}$ Hz, and $\Delta\omega_2 = 5^{1/6} \times 10^{14}$ Hz. Note that the symmetric spectral shape in frequency corresponds to an asymmetric shape in wavelength, as shown in Fig. 1(a). A Gaussian spectrum (dotted curve) with the same FWHM (103.77 nm) with the spectral density function as

$$|S(\omega)|^2 = \exp\left[-\frac{(\omega - \omega_0)^2}{{\Delta\omega_3}^2}\right], \tag{9}$$

is assumed for comparison, where $\Delta\omega_3 = 1.98 \times 10^{14}$ Hz. The normalized interference fringe envelopes can be obtained with the Fourier transforms of the spectral density functions. Their numerical results are shown in Fig. 1(b) with the dashed and dotted curves for the non-Gaussian and Gaussian cases, respectively, and both are dispersion matched. It can be seen that the FWHM of the autocorrelation function of the non-Gaussian case (1.8 μm) is smaller than that of the Gaussian case (2.52 μm). The solid curve in Fig. 1(b) shows the result (approximately 1.06 μm) when a proper dispersion mismatch [$a = 6 \times 10^{-30}$ sec^2 and $b = 0$ in Eq. (5)] is included. Here, the FWHM of the autocorrelation function is further reduced. However, significant sidelobes appear in the autocorrelation function, which is consistent with previously reported Ref. 14. In this paper we experimentally implemented the FWHM reduction of the autocorrelation function and improved the OCT resolution with an image-retrieval algorithm.

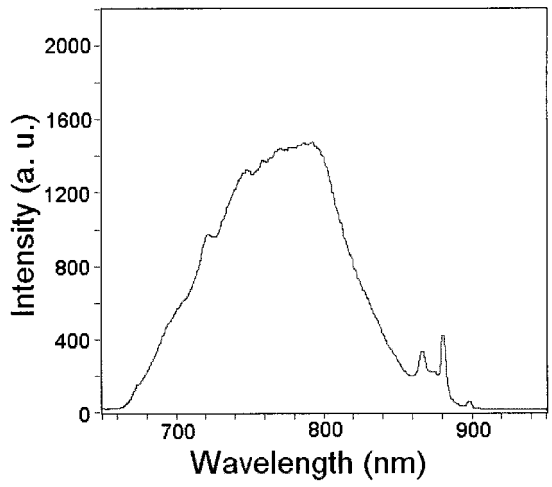

Fig. 3. Spectrum of the laser used for the OCT system.

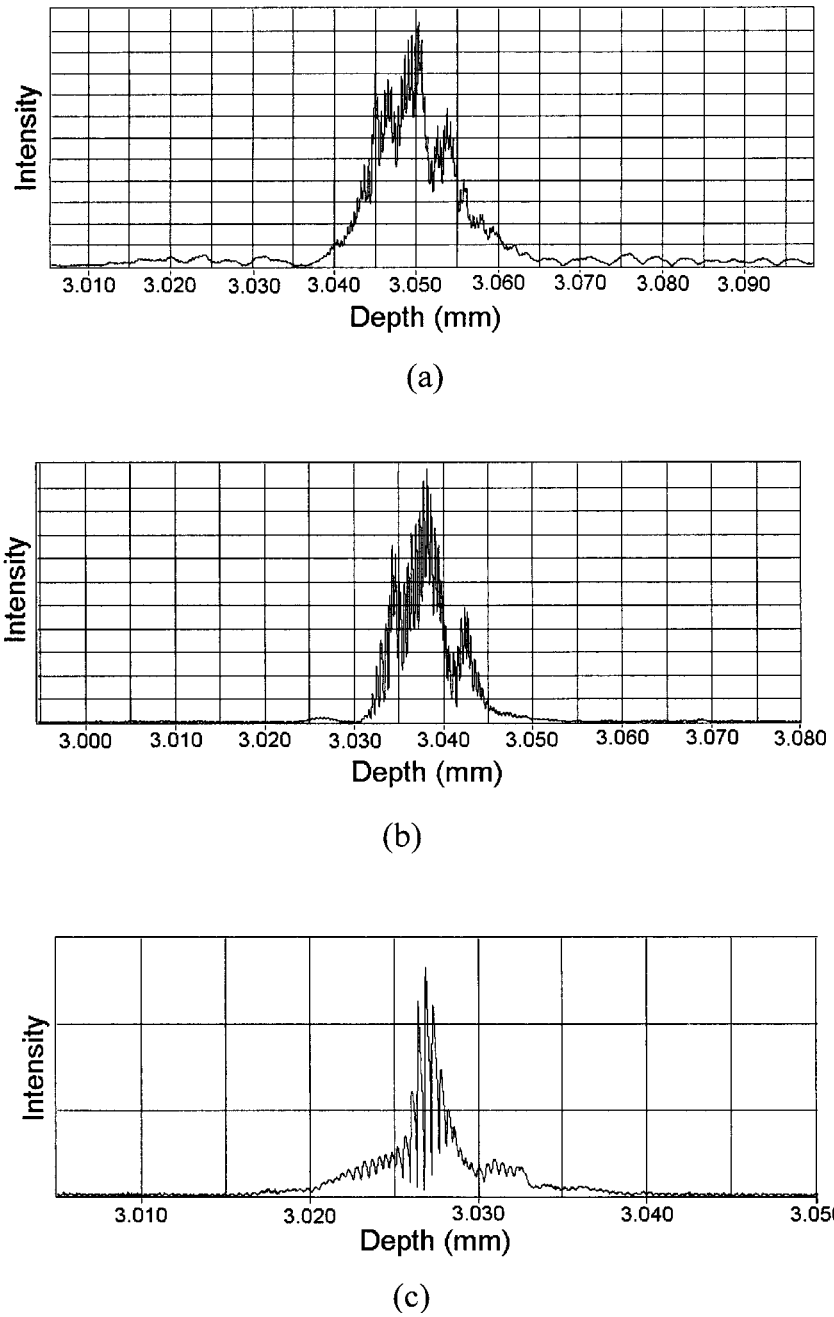

Fig. 4. Interference fringe patterns of the OCT system in the cases: (a) without dispersion compensation, (b) and (c) with dispersion manipulation when four and eight glass slides are used, respectively.

3. Experimental Procedures

The experimental setup consisted of a typical free-space OCT system as shown in Fig. 2. The light source was a solid-state laser pumped, mode-locked Ti:sapphire laser (femtosource), providing 10 to 12 fs pulses at 76 MHz. The corresponding spectrum is shown in Fig. 3. The FWHM of the spectrum was approximately 100 nm. The spectral shape is obviously non-Gaussian. A constant-speed translation stage was used in the reference arm for phase modulation and depth scanning. After a photodetector, OCT signals were digitized and processed on a computer. Without dispersion manipulation, the demodulated interference fringe pattern of the front surface of a glass slide is shown in Fig. 4(a), in which a multiple-peak feature of approximately 10 μm in FWHM can be observed. The multiple-peak feature of the interference fringe pattern is supposed to come from the dispersion mismatch between the reference and the sample arms and possibly the non-Gaussian spectral shape. The dispersion mismatch may originate from the use of the beam splitter and focal lenses in the interferometer. To implement dispersion manipulation, a stack of glass slides, usually

used with a microscope, with a thickness of 1.1 mm each, was inserted into the reference arm. The interference fringe pattern was changed with the number of glass slides employed. Fig. 4(b) shows the result when four slides were used. This fringe pattern has a FWHM of approximately 6 μm. Fig. 4(c) shows the result when eight slides were used. This fringe pattern has a FWHM of only approximately 1.7 μm. However, it consists of quite significant tails. According to the interference fringe patterns, none of the signals shown in Fig. 4 corresponds to the case of dispersion balance. Note that in using the glass slides in the reference arm, we could not be sure whether the dispersion mismatch was enhanced or reduced.

4. Retrieval Algorithm

To reduce the effects of the fringe tails on OCT scanning images, we propose a computer algorithm based on the following principles: First, an OCT image can be regarded as the superposition of fringe envelopes pixel-by-pixel with various intensities, which depend on sample structures. This concept is demonstrated with the equation as

$$I(z) = \int_{z_i}^{z_f} I'(z') f(z - z') \mathrm{d}z'. \tag{10}$$

Here, I' represents the backscattered intensity and f stands for the normalized interference fringe envelope, which symbolizes the envelope of the oscillatory distribution in Fig. 4(c). After the convolution shown in Eq. (10), I represents the detected signal, which is supposed to originate from depth z. Here, z_i and z_f denote the appropriate integration limits. In the real operation, data of pixels were collected and the integral in Eq. (10) is replaced with a summation as

$$I(i) = \sum_{j=1}^{N} I'(j) f(i - j) \Delta z, \tag{11}$$

where N is the assumed pixel number and Δz is the pixel size of the OCT system.

We developed a computer algorithm based on an iteration method to retrieve the backscattered intensity distribution $I'(i)$, which represents the sample structure. Figure 5 shows the flow chart of the computer algorithm. We used a single reflection from a glass slide to obtain the interference fringe envelope. The normalized interference fringe envelope function f was the average of ten measurements and normalized to unity at the zero position. We used the detected signal $I(i)$ multiplied by a factor $2/(M + m)$ as the initial trial function $I'(i)$, where M and m are the maximum and minimum values of function $r(i)$ defined as

$$r(i) = \sum_{j=1}^{N} \frac{I(j) f(i - j)}{I(i)}. \tag{12}$$

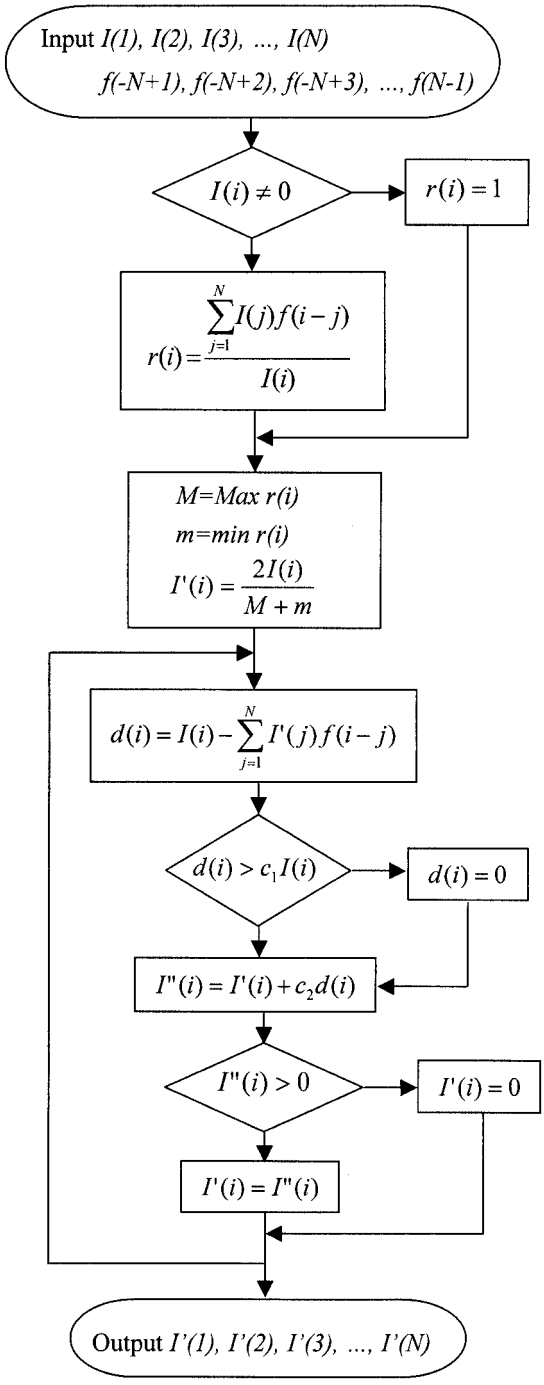

Fig. 5. Flow chart of the retrieval algorithm.

We compared the detected intensity $I(i)$ to the convolution of the trial function $I'(i)$ and the normalized interference fringe envelope function f, and obtained the difference between them at each pixel $d(i)$. We neglected the difference when it was smaller than $I(i)$ multiplied by a factor c_1, because small computer inaccuracies might be generated during the process and result in noise. The proper value of c_1 was estimated to be 0.001. The difference $d(i)$ was then multiplied by a factor c_2 and added to the original trial function $I'(i)$ to obtain a new function $I''(i)$. The

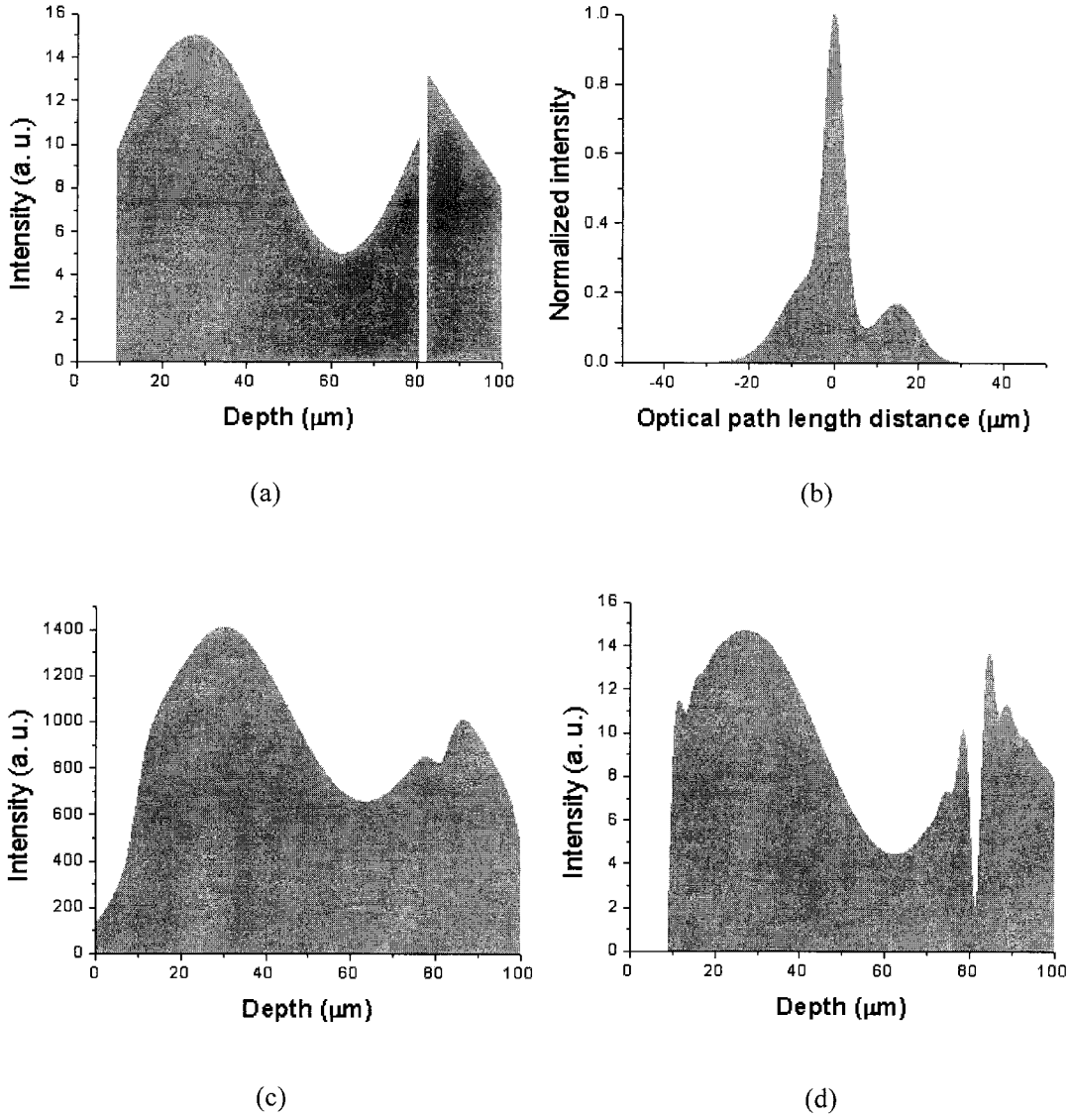

Fig. 6. Simulation results of scanning a phantom structure: (a) assumed backscattered intensity distribution or phantom structure, (b) assumed interference fringe envelope, (c) measured intensity distribution of an OCT system with the interference fringe envelope function shown in (b), and (d) retrieved phantom structure after 100 iterations of the proposed algorithm.

factor c_2 was used to adjust the retrieving speed of the program. A larger value of c_2 resulted in a higher retrieving speed; however, the process would not approach to a stable solution when the value of c_2 was too large. A suitable value of c_2 was $1/0.055N$ based on our experience. The new trial function was obtained by replacing the negative values of $I''(i)$ with 0. Such a process was iterated until the processed image was satisfactory. Note that an OCT signal corresponds to the object structure convolved with the interferometric signal (with the fringe pattern). When the spacing between two features is smaller than the coherence length, the two interferometric signals considerably overlap, and the relative phase of the fringes has to be taken into account in the retrieval procedure. However, because the major goal of the current retrieval algorithm is to reduce the sidelobe effects,

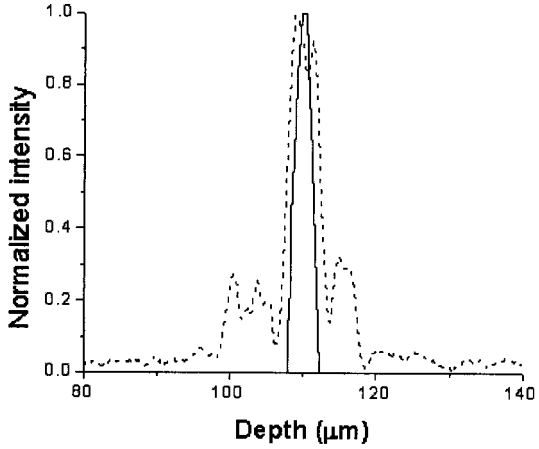

Fig. 7. One-dimensional backwardscattered intensity distribution of the OCT image of a glass slide before processing (dashed curve) and after processing (solid curve).

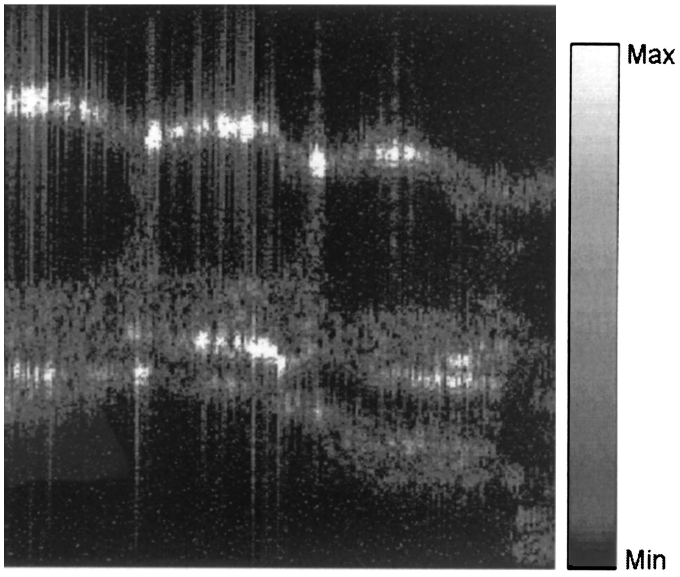

(a)

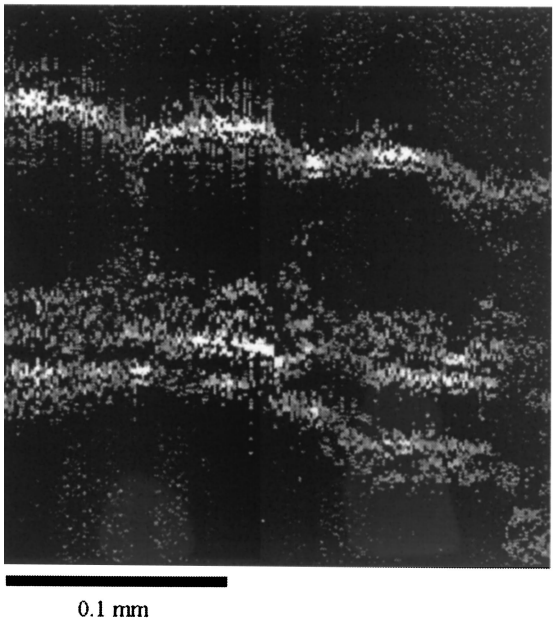

(b)

Fig. 8. OCT images of onion cells of the cases: (a) before processing and (b) after processing.

the inclusion of phase for further resolution improvement will be left for further research.

5. Results of Image Quality Improvement

To demonstrate the feasibility of this algorithm, we conducted the following simulation. Figure 6(a) shows the backscattered intensity distribution of a phantom structure. Note that sharp boundaries at both ends and a sharp depression were assumed to demonstrate the retrieving capability of the proposed algorithm. From OCT scanning with the fringe envelope function shown in Fig. 6(b), the detected intensity distribution is shown in Fig. 6(c). Here, one can see that the original sharp features disappear. This signal distribution was processed with the procedure described in Fig. 5 to retrieve the backscattered intensity distribution. The result after 100 iterations is shown in Fig. 6(d), in which the original sharp features are essentially recovered although there exist oscillations near the sharp boundaries. More iterations are required to approach the real structure. The result in Fig. 6(d) provides us with confidence in using the proposed algorithm.

For demonstrating the capability of the proposed

algorithm in a real OCT operation, we used a glass slide and an onion sample as the scanning objects. Figure 7 shows the one-dimensional backscattered intensity distribution of the scanning image and the processed image after 100 iterations of the glass slide. The dashed line depicts the raw data and the solid line depicts the processed data. One can see that the fringe tails are tremendously suppressed and the FWHM of the signal profile is reduced after the process. Figure 8(a) shows the scanning image of an onion sample when eight glass slides were inserted into the reference arm for dispersion manipulation. Although the structures of onion cells can be recognized, the effects of fringe tails (spiky features in the figure) did blur the image and reduce the spatial resolution. This image was then processed with the proposed algorithm. After 100 iterations of the retrieval procedure, the image quality has been improved, as shown in Fig. 8(b). The spiky features are now tremendously suppressed and the image contrast is enhanced. Particularly, the layered structures near cell walls can now be clearly seen.

It was estimated that the required process time for 100 iterations of a depth scan of 1000 pixels was shorter than 0.25 s. The required process time of a frame of 1000 $\times$ 200 pixels (1 mm in depth by 1 mm in width) should be shorter than one min. With such a process speed, we cannot claim a real-time operation. Although in terms of speed, this process procedure cannot compete with a real-time scanning OCT system, which has a frame rate of 8–10 Hz,[15,16] it is acceptable in certain applications. Development of software should result in a faster process.

6. Conclusions

In summary, we have demonstrated what to our knowledge is a novel technique of improving the spatial resolution of an OCT system given a certain light source spectrum that was not well shaped. By inserting dispersive materials into the reference arm of the OCT system, the resultant dispersion manipulation led to a FWHM of the interference fringe envelope smaller than the Fourier transform-limited value of a Gaussian spectral shape with the same spectral FWHM, at the expense of significant tails. Such tails would blur OCT images if their effects were not removed. In the proposed technique, the tail effects were tremendously reduced with a retrieval algorithm. Simulation results and OCT real scanning images have shown the promising capability of the proposed technique.

This research was supported by National Health Research Institute, Taiwan, under the grant of NHRI-GT-EX89E819L.

References

1. D. Huang, E. A. Swanson, C. P. Lin, J. S. Schuman, W. G. Stinson, W. Chang, M. R. Hee, T. Flotte, K. Gregory, C. A. Puliafito, and J. G. Fugimoto, "Optical coherence tomography," Science **254,** 1178–1181 (1991).
2. G. J. Tearney, M. E. Brezinski, B. E. Bouma, S. A. Boppart, C. Pitris, J. F. Southern, and J. G. Fujimoto, "In vivo endoscopic optical biopsy with optical coherence tomography," Science **276,** 2037–2039 (1997).
3. Y. Pan, H. Xie, and G. K. Fedder, "Endoscopic optical coherence tomography based on a microelectromechanical mirror," Opt. Lett. **26,** 1966–1968 (2001).
4. C. E. Saxer, J. F. de Boer, B. H. Park, Y. Zhao, Z. Chen, and J. S. Nelson, "High-speed fiber-based polarization-sensitive optical coherence tomography of *in vivo* human skin," Opt. Lett. **25,** 1355–1357 (2000).
5. W. Drexler, U. Morgner, F. X. Kärtner, C. Pitris, S. A. Boppart, X. D. Li, E. P. Ippen, and J. G. Fujimoto, "*In vivo* ultrahigh-resolution optical coherence tomography," Opt. Lett. **24,** 1221–1223 (1999).
6. T. A. Birks, W. J. Wadsworth, and P. St. J. Russel, "Supercontinuum generation in tapered fibers," Opt. Lett. **25,** 1415–1417 (2000).
7. I. Hartl, X. D. Li, C. Chudoba, R. K. Ghanta, T. H. Ko, J. G. Fujimoto, J. K. Ranka, and R. S. Windeler, "Ultrahigh-resolution optical coherence tomography using continuum generation in an air-silica microstructure optical fiber," Opt. Lett. **26,** 608–610 (2001).
8. A. M. Kowalevicz, T. Ko, I. Hartl, J. G. Fujimoto, M. Pollnau, and R. P. Salathé, "Ultrahigh resolution optical coherence tomography using a superluminescent light source," Opt. Express **10,** 349–353 (2002).
9. E. A. Swanson, D. Huang, M. R. Hee, J. G. Fujimoto, C. P. Lin, and C. A. Puliafito, "High-speed optical coherence domain reflectometry," Opt. Lett. **17,** 151–153 (1992).
10. M. D. Kulkarni, C. W. Thomas, and J. A. Izatt, "Image enhancement in optical coherence tomography using deconvolution," Electron. Lett. **33,** 1365–1367 (1997).
11. M. Bashkansky, M. D. Duncan, and J. Reintjes, "Engineering and laboratory notes—Signal processing for improving field cross-correlation function in optical coherence tomography," Appl. Opt. **37,** 8137–8138 (1998).
12. R. Tripathi, N. Nassif, J. S. Nelson, B. H. Park, and J. F. de Boer, "Spectral shaping for non-Gaussian source spectra in optical coherence tomography," Opt. Lett. **27,** 406–408 (2002).
13. B. L. Danielson and C. Y. Boisrobert, "Absolute optical ranging using low coherence interferometry," Appl. Opt. **30,** 2975–2979 (1991).
14. C. K. Hitzenberger, A. Baumgartner, and A. F. Fercher, "Dispersion induced multiple signal peak splitting in partial coherence interferometry," Opt. Commun. **154,** 179–185 (1998).
15. V. Westphal, S. Yazdanfar, A. M. Rollins, and J. A. Izatt, "Real-time, high velocity-resolution color Doppler optical coherence tomography," Opt. Lett. **27,** 34–36 (2002).
16. Y. Zhao, Z. Chen, Z. Ding, H. Ren, and J. S. Nelson, "Real-time phase-resolved functional optical coherence tomography by use of optical Hilbert transformation," Opt. Lett. **27,** 98–100 (2002).